Field-assisted oxidation of rhodium

J.-S. McEwen [a,*], P. Gaspard [a], F. Mittendorfer [b], T. Visart de Bocarmé [c], N. Kruse [c]

[a] *Centre for Nonlinear Phenomena and Complex Systems, Campus Plaine - CP 231, Université Libre de Bruxelles, B-1050 Brussels - Belgium*

[b] *Faculty of Physics, Universität Wien, and Centre for Computational Materials Science Sensengasse 8/12 A-1090 Wien, Austria*

[c] *Chemical Physics of Materials, Campus Plaine - CP 243, Université Libre de Bruxelles, B-1050 Brussels - Belgium*

Abstract

The oxidation of nanosized rhodium facets is investigated in the presence of a high external electric field with field ion microscopy experiments (FIM). Corresponding density functional theory (DFT) calculations were done on Rh(001), Rh(011) and Rh(111). A cross-like granular structure is obtained with FIM when the electric field is increased from 11 V/nm to 12.3 V/nm, which strongly indicates that the field promotes the oxidation of the tip. The DFT calculations confirm this scenario with a corresponding reduction of the activation barrier for oxygen incorporation into the surface of an oxide layer.

1 Introduction

Despite the large number of studies on oxide formation at transition metal surfaces in the literature, the actual processes involved in their initial formation is an open and active field. Although there is a general agreement that the mechanistic steps leading to oxide formation involve the dissociative adsorption of oxygen on the metal surface, no standardized model could be worked out so far for the lattice penetration of atomic oxygen and its aggregation to an amorphous oxide finally crystallizing into stoichiometric bulk oxide phases. Recently, surface oxides have received a lot of attention as a possible precursor to the bulk oxide phase. Surface oxides have also been argued to have

* Corresponding author. Tel: +32-2-650-5798; fax: +32-2-650-5767.
Email address: jmcewen@ulb.ac.be (J.-S. McEwen).

unique properties [1] and the stability of various surface oxides on rhodium single crystals has been studied in great detail [2–5]. In these studies, scanning tunneling microscopy experiments (STM) along with supporting density functional theory (DFT) calculations have led to the observation of a RhO_2 surface oxide trilayer on Rh(001), Rh(011) and Rh(111) surfaces which differs from the Rh_2O_3 stoichiometry that one encounters in the bulk oxide. The kinetics of the reduction of the surface oxide were studied on Rh(111) and Rh(011) as well [6,7]. However, no attempt has been undertaken to clarify which atomistic steps are needed to obtain a surface oxide from a saturated adsorbed layer of oxygen. Other studies in the oxide formation on rhodium crystals have been undertaken with the field ion microscope (FIM) in which an external electric field is applied to a metal tip, of the order of ten Volts per nanometer [8]. This technique can also be combined with pulsed field desorption mass spectroscopy to obtain local chemical information [9]. These electric fields are ubiquitous and encountered at any metal surface due to charge separation [10]. They can be examined experimentally with field emission techniques [11] and, on semiconductor surfaces, some investigations were undertaken with STM [12]. Theoretically, the works of H.J. Kreuzer were among the first to study field-induced adsorption and desorption with quantum mechanical calculations [13,14]. Besides these works, the effect of strong electric fields on clean metal surfaces was also investigated by DFT [15,16]. The interaction of an electric field with surface dipoles due to oxygen-metal bonds is crucial for the understanding of the very initial stages leading to oxidation. Moreover, subsurface oxygen has been also determined to play a role in the feedback mechanism of the oscillating CO oxidation on Pd(110) [17]. In field ion microscopy experiments of the oxygen-hydrogen reaction on rhodium tips, oxygen subsurface diffusion seems to occur likewise and involved in the nonlinear reaction behavior [9]. Interestingly, no oscillatory behavior has been observed on extended rhodium single surfaces of uniform orientation making it possible that the electric field plays a fundamental role in the formation of subsurface oxygen. Indeed, when strong enough electric fields are applied they can induce a re-arrangement of the electronic orbitals and can lead to new phenomena which cannot be simply obtained by increasing the oxygen pressure or the temperature of the adsorbate. In this letter, we combine field ion microscopy experiments with density functional theory calculations to show that an externally applied electric field indeed diminishes the energetic barrier in the incorporation of oxygen into the metal.

2 Results and discussion

We begin with our FIM experiments to investigate the reaction of oxygen with rhodium tips. This allows the extremity of a tip, with a nanometric radius of

curvature ($\sim$ 20 to 30 nm), to be imaged giving simultaneously a variety of crystallographic orientations with atomic resolution [18]. The sample can be exposed to reactive gases at high temperatures, up to 900 K, and dynamic phenomena can be followed directly by video-FIM. The present study aims at proving that rhodium surface oxidation is highly sensitive to an external electric field the value of which can be finely tuned in FIM studies. Surface oxidation and reduction can be followed by using oxygen and hydrogen respectively, and to a further extent, a well chosen mixture of these two gases. Under these conditions the catalytic formation of water can also be monitored [9]. At temperatures ranging between 400 and 500 K, surface oxidation is seen to occur on the (001) plane and on zone lines between the latter and {011} orientations. Above 525 K, the surface sensitivity towards oxidation is much less pronounced. Earlier FIM studies have shown that surface Rh oxides appear as granules of high brightness [8]. The same structure is also visible when low amounts of hydrogen, insufficient to provoke the reduction of the oxide layer, are added to oxygen gas in the FIM chamber. At higher H_2 pressures, fast removal of the oxide layer is observed on specific regions of the tip apex along with a dramatic modification of the local patterns unravelling the structure and the symmetry of a metallic surface. In the present work, we focused our attention on the Rh(001) plane. Figure 1c shows a field ion micrograph of a Rh tip imaged with atomic resolution at 50 K and 35 V/nm. From this reference state, the sample was heated to 450 K and O_2 was admitted in the chamber at 5×10^{-4} Pa. The field was tuned to 11 V/nm, sufficient for image formation to occur. Under these conditions, the pattern was associated with an oxidized surface. The hydrogen pressure was slowly raised up to 5.7×10^{-3} Pa to trigger the transition towards the metallic state, as presented in Fig. 1a. Under these conditions, the pattern is stable and does not show a reverse transition towards the initial oxidized surface state. Despite a quite poor lateral resolution at this temperature, the main features of initial Rh tip are still visible. Increasing the field from 11 to 12.3 V/nm directly leads to the formation of a cross-like feature covering the four {011} planes and the topmost (001) layer (Fig. 1b). The pattern exhibits the granular structure associated with an oxidized state. It is noteworthy that the gas supply function on the tip apex in FIM is dependent on the external electric field, i.e. on the interaction of this field with polarizable molecules like of O_2 and H_2 [19]. As a consequence, the local partial pressures of O_2 and H_2 directly above the tip apex increase by 20 % and 14 %, respectively, when the field is raised from 11 to 12.3 V/nm [19]. However, the hydrogen pressure has to be increased by some 400 % in order to keep the surface in the metallic state during oxygen/hydrogen co-adsorption at 12.3 V/nm. Therefore, the pressure increase due to the electric field cannot be the sole effect that explains the results reported here. One further possible effect is the decrease of the activation energy for the oxidation of the surface, which we consider in this letter.

To gain an atomistic understanding of this phenomenon, DFT calculations

were performed with the Vienna ab initio simulation package (VASP) [20–22], a plane-wave DFT program which is based on the projector augmented wave method [23]. A cut-off energy for the expansion of the plane waves of 250 eV was found to be sufficient for an accurate calculation of the binding energy. The nudged elastic band method was applied when calculating the activation energies [24]. The Brillouin zone was sampled by a grid of $(16\times16\times1)$ k-points Monkhost-Pack grid for a (1×1) cell and was reduced according to the size of the unit cell.

There are many possible processes that can lead to the reduction of the observed surface oxides on rhodium. In this letter we have considered a stepwise reduction of the c(2×8) trilayer O-Rh-O surface oxide on the Rh(001) surface [3], by removing oxygen atoms successively. In particular, we consider a hopping mechanism of an oxygen atom to go from the inner oxygen layer to the outer one that could occur during the fluctuations when the c(2×8) surface oxide is almost complete. Our initial state has an oxygen vacancy in the outer oxygen layer, which we denote as a trilayer−O structure [meaning an oxygen atom is missing in the c(2×8) trilayer]. On the other hand, the final state has a vacancy in the inner oxygen layer of the c(2×8) surface oxide, in the following noted as trilayer−O_s structure (where $-O_s$ denotes a subsurface oxygen vacancy). The trilayer−O structure is found to be significantly less stable than the trilayer−O_s structure, with a total energy difference of 0.78 eV. Thus, even at a coverage close to 2 ML, oxygen vacancies in the uppermost oxygen layer are energetically unstable, and will be filled with subsurface oxygen.

We find that this observation also holds upon a further reduction of the oxide film. In particular, we calculated the energy difference between a situation with two nearest neighbor vacancies in the inner layer [denoted henceforth as the trilayer−$(2O_s)$] with respect to when both the outer and the inner oxygen layers have a vacancy at nearest neighbor distances of each other [i.e., a trilayer−(O_s+O) structure, which is partly depicted in Fig. 1 d]. Again we find that with a difference of 0.60 eV the configuration with both vacancies in the inner oxygen layer [trilayer−$(2O_s)$] is significantly more stable than the configuration with mixed vacancy sites [trilayer−(O_s+O)]. However, in this letter we are primarily interested in the influence of the electric field on the binding energy differences for low Miller index surfaces [Rh(001), Rh(011) and Rh(111)]. More precisely, in addition to the surface oxide on Rh(100) discussed above we have considered the c(2×4) trilayer O-Rh-O surface oxide on the Rh(011) surface, which has been observed with STM experiments [4]. The initial state configuration has two oxygen vacancies in the inner oxygen layer while our final state has one vacancy in the outer and another in the inner oxygen layer. Finally, when calculating the energy barrier on the Rh(111), we have considered a $(\sqrt{3} \times \sqrt{3})R30^\circ$ O-Rh-O trilayer surface oxide in a p(2x2) supercell, which has been shown to be very similar to the (9×9) trilayer O-Rh-O surface oxide that has been observed experimentally [2], in order to

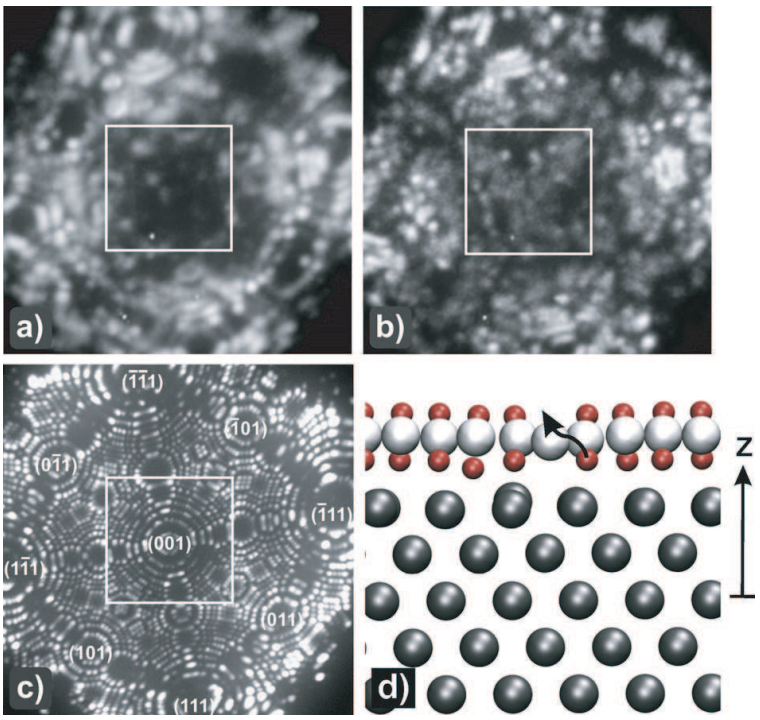

Fig. 1. (a) Field ion patterns exposed to a hydrogen rich H_2+O_2 gas mixture (P_{H_2} = 5.7×10^{-3} Pa, P_{O_2} = 5×10^{-4} Pa) at T = 450 K, F = 11 V/nm. The white square acts as a guide-to-the-eye to follow the patterns on the (001) plane. (b) Same as in (a) but F = 12.3 V/nm. Field values are determined from the field ion micrograph of a rhodium tip given in (c) where the best imaging voltage is associated with a field of 35 V/nm in which atomic resolution is obtained. Other image conditions: P_{Ne} = 10^{-3} Pa, T = 50 K. (d) The initial configuration on Rh(001) in the DFT calculations. The arrow beginning from an oxygen atom indicates the reaction pathway starting from the inner oxygen layer to the outer one. The value of z is relative to the position of the closest fixed rhodium layer of the underlying substrate. The grey spheres are rhodium atoms, the white spheres are rhodium atoms in the oxide layer, while the small grey spheres (red online) are oxygen atoms.

keep the calculation of the energy barrier computationally manageable. Here we also had two oxygen vacancies in our initial and our final states (two in the inner layer compared to one in the outer and another in the inner oxygen layer).

The reaction path can be defined by the movement of an oxygen atom. In the calculation of the energy barriers, we additionally fixed the z position of this oxygen atom for the various intermediate configurations. The corresponding energy barriers are depicted in Fig. 2. The z position of the transition state is situated in all cases near the rhodium layer position within the oxide. As shown in Fig. 2, the hopping barrier between the lower and upper oxygen layers is the largest for the Rh(011) surface and the smallest for the Rh(111) surface. This observation can be explained by a simple sterical argument, as the average Rh-Rh distance within the oxide layer is the largest for our model

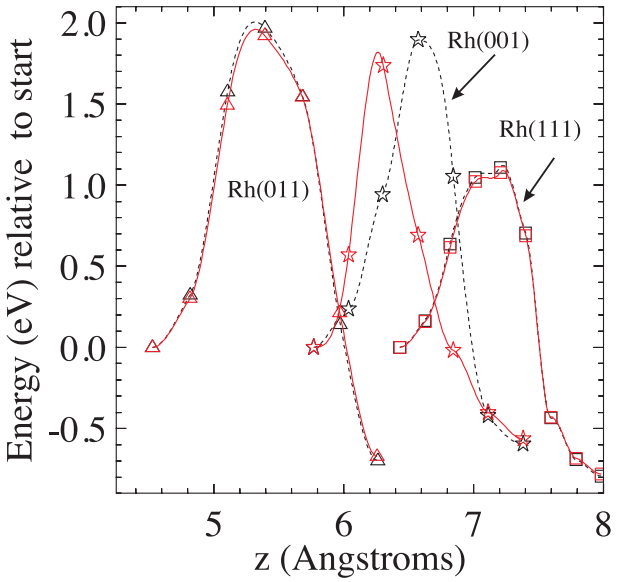

Fig. 2. The hopping barrier for an oxygen atom to go from the inner to the outer oxygen layer (increasing z) within a surface trilayer oxide with two oxygen vacancies on an underlying Rh(001) (stars), Rh(011) (triangles) and a Rh(111) (squares) substrate using the generalized gradient approximation (GGA) according to Perdew et al. [30]. The surface was modelled with slabs consisting of five rhodium layers with the bottom three layers fixed at the theoretical bulk lattice constants of a=3.844 Å . The vacuum thickness was at least $\sim$ 11 Å. The continuous lines are cubic spline interpolations between the intermediate values at an electric field of 4 V/nm (solid lines) and 0 V/nm (dotted lines).

of the Rh(111) oxide (with a density of 11.7 Rh atoms/nm^2), followed by Rh(001) (11.8 atoms/nm^2) and finally the smallest distance for Rh(011) (12.0 atoms/nm^2). Nevertheless, the low barrier on Rh(111) might be due to our simplified p(2×2) model; for the experimental (9×9) structure the resulting barrier might be significantly higher not only because of its larger rhodium atom density in the trilayer (12.3 atoms/nm^2) but also because the number of oxygen atoms is higher in such a larger cell. Indeed, the (9×9) cell with a full oxide layer contains 128 oxygen atoms although the smaller p(2×2) cell would contain 6 oxygen atoms. Since we remove two oxygen atoms from the surface oxide to form our model system, the change in the number of oxygen atoms would be from 128 to 126 in the experimental (9×9) cell, but is from 6 to 4 in our simplified model. Hence, if we assume that the barrier height is proportional to the change in the number of oxygen atoms, the barrier will be significantly reduced in our p(2×2) model, as we observe.

In the final step we have investigated the influence of an electrical field on the reaction barriers. As the convergence of the calculations is considerably hindered by a strong electric field, we have only simulated a moderate electric field of 4 V/nm instead of the experimental values of 10 V/nm. The reason for this slow convergence is that when a field separates electronic from ionic

Table 1
The activation energies at a vanishing field value (eV) and the resulting change for an applied electric field $F = 4$ V/nm using the nudged elastic band method [24]. We note that -$E^{\ddagger}_{\rm in}$/F and -$E^{\ddagger}_{\rm out}$/F reflect the corresponding dipole moments. The extrapolated activation energies at experimental field values are also shown.

Surface	Rh(001)	Rh(011)	Rh(111)
$E^{\ddagger}_{\rm in}(F = 0$ V/nm)	2.490	2.702	1.914
$E^{\ddagger}_{\rm out}(F = 0$ V/nm)	1.895	2.004	1.121
$\Delta E^{\ddagger}_{\rm in}$ (eV)	$-0.027\ F$	$-0.018\ F$	$-0.011\ F$
$\Delta E^{\ddagger}_{\rm out}$ (eV)	$-0.018\ F$	$-0.011\ F$	$-0.008\ F$
$E^{\ddagger}_{\rm in}(F = 11$ V/nm)	2.193	2.504	1.793
$E^{\ddagger}_{\rm out}(F = 11$ V/nm)	1.697	1.883	1.033
$E^{\ddagger}_{\rm in}(F = 12.3$ V/nm)	2.158	2.481	1.779
$E^{\ddagger}_{\rm out}(F = 12.3$ V/nm)	1.673	1.868	1.023

charges from the surface, large restoring forces associated with this separation can overshoot from iteration to iteration [25].

The influence of an external electric field of 4 V/nm on the energetic barriers is shown as solid lines in Fig. 2. In all cases, the hopping barrier for an oxygen atom to go from the outer oxygen layer to the transition state ($E^{\ddagger}_{\rm in}$) is diminished in the presence of an external electric field. Similarly, the hopping barrier for an oxygen atom to go from the inner oxygen layer to the transition state ($E^{\ddagger}_{\rm out}$) is also reduced in the presence of a field, but not as significantly. The values of these barriers are shown in Table 1 for all three surfaces in the absence of a field. The electric field also results in an earlier barrier on the Rh(001) surface. Finally, we remark that the relative energy differences between the initial and the final states are smaller in the presence of an external field. This can be intuitively expected since the electric field dies out as one goes into the slab, which causes an unequal change in the energies.

Assuming a monotonic dependence for both barriers, which has been obtained in a previous study for the desorption energy of oxygen on gold [26], we have also deduced their effective dipole moments. They are given in Table 1, which shows that the largest change of the activation barrier is obtained for the Rh(001) surface. These dipole moment values should also be taken into account in any kinetic model in which all the different orientations of the tip are included [27]. Finally, using these dipole moment values, the resulting activation barriers at the experimental field values are deduced and given in Table 1. However, we note that the field will induce changes of the electron density

that are nonlinear [13,14]. Such effects could also play a role in the appearance of a cross-like granular structure when changing the electric field by only 1.3 V/nm.

The resulting reduced barrier with a higher electric field can be understood intuitively by a simple physical picture. Indeed, since the oxygen atom is more electronegative than the rhodium atom, it carries a partial negative charge so that the respective surface dipole has the wrong orientation with respect to the electric field vector. Classically, this results in a torsional moment that pushes the oxygen atom subsurface.

The influence of an external field on the thermodynamic phase diagrams [2] can also be correlated to the results obtained above. Let us consider in particular the Rh(001) surface and define the adsorption energy for an applied electric field F as $E_{\rm ads}(F) = -\{E_{\rm tot}(F) - E_{\rm Rh(001)}(F) - N_{\rm O}[E_{\rm O}(F) - D_e(F)/2]\}/N_{\rm O}$, where $E_{\rm tot}(F)$ is the total energy for the calculated cell, $N_{\rm O}$ is the number of oxygen atoms in the cell, $E_{\rm Rh(001)}(F)$ is the energy of a clean Rh(001) surface, $E_{\rm O}(F)$ is the energy of an isolated oxygen atom and $D_e(F)$ is the dissociation energy of an O_2 molecule. The change in the Gibbs free energy of adsorption is then obtained using [28]

$$\Delta G = [N_{\rm O}E_{\rm ads} + N_{\rm O}\Delta\mu_{\rm O}(T,p) + \mu_{\rm Rh}\Delta N_{\rm Rh}]/(A/A_0) \qquad (1)$$

where $\Delta\mu_{\rm O}(T,p) = \mu_{\rm O}(T,p,F=0) - [E_{\rm O}(F) - D_e(F)/2]$ is the chemical potential with respect to the energy of an isolated O_2 molecule as reference zero, $p = P_{\rm O_2}$ is the pressure of oxygen and factor A/A_0 is the area of the surface if the cell divided by the surface area of a (1×1) cell. Finally, $\mu_{\rm Rh}\Delta N_{\rm Rh}$ is non-zero only if the total number of metal atoms in the oxide is different to clean surface and $\mu_{\rm Rh}$ is taken to be the binding energy of Rh in the bulk.

The change in Gibbs free energy per unit cell depicted in Fig. 3 shows a decrease when an external field is applied. Moreover, the energy difference between the initial [trilayer−(O_s+O)] and the final state [trilayer−($2O_s$)], changes by $30/(A/A_0)$ meV when the electric field is switched on. We also show a corresponding pressure scale in Fig. 3, which is obtained via the ideal gas formula, $\mu_{\rm O}(T,p) = \mu_{\rm O}(T,p_0) + (1/2)k_{\rm B}T\ln(p/p_0)$. We remark that the Gibbs free energy similarly changes if the chemical potential or pressure are shifted. The dependence of the theoretical phase diagram on the electric field could also result in a corresponding displacement of the surface phase transitions between various adsorbate structures at different coverages. Moreover, it should change the equilibrium shape of a crystal since the stability of various surface orientations was found to depend on the external electric field in FIM experiments [8].

Looking for an atomistic mechanism of oxidation, Fig. 3 can give us indications

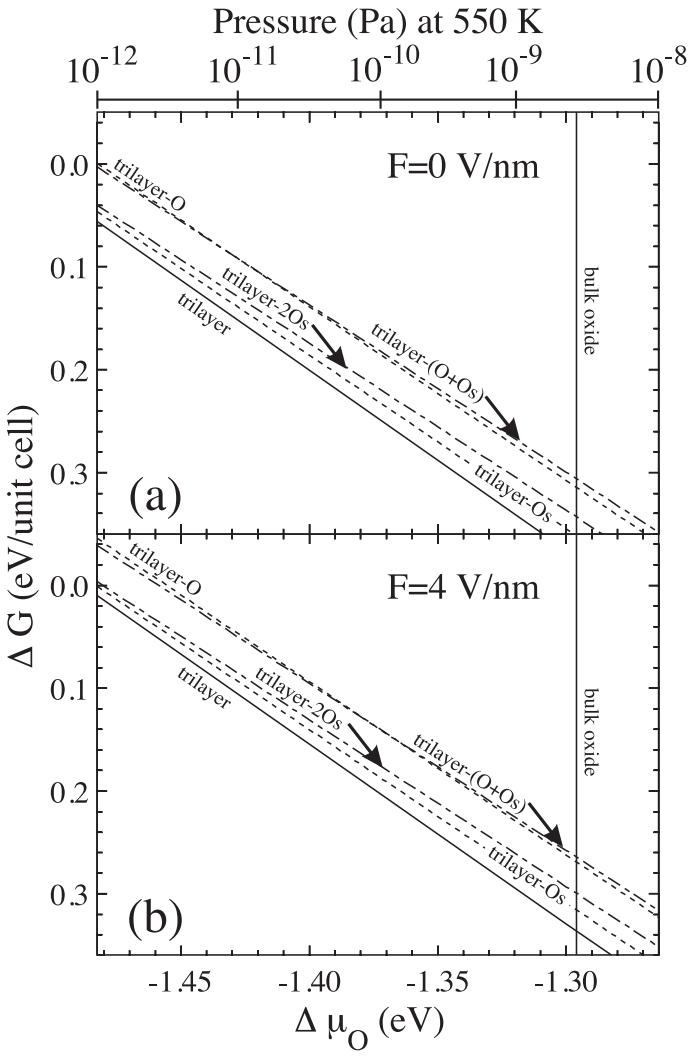

Fig. 3. (a) The change in the Gibbs free energy of adsorption, as given by Eq. (1), as a function of the chemical potential for several oxide phases on a Rh(001) surface at a vanishing electric field value for the trilayer (solid lines), trilayer−O (dotted lines), trilayer−O_s (dotted lines), trilayer−($2O_s$) (dash-dotted lines) and trilayer−(O_s+O) (dash-dotted lines) surface oxides. (b) The Gibbs free energy of adsorption for the same oxide phases at a field value of 4 V/nm. The corresponding pressure scale is also shown at 550 K.

Table 2
Defect energies (difference in ΔG [eV/supercell] of Gibbs free energies between the ideal Rh(100) surface oxide and the reduced oxides) in the absence of an electric field at the experimental conditions ($\mu = -0.8$ eV, $P_{O_2} = 5 \times 10^{-4}$ Pa and $T = 450$ K) and at $\mu = 0$ eV.

	trilayer−O_s	trilayer−O	trilayer−$2O_s$	trilayer−(O+O_s)
$\Delta G(\mu = -0.8$ eV)	0.82	1.58	1.60	2.20
$\Delta G(\mu = 0)$	1.63	2.38	3.20	3.80

on how the surface oxide may be formed. Following the minimum path of the free energy, it is evident that the stable configurations of the reduced surface oxides are the ones with oxygen atoms missing in the inner layer instead of the outer one. This is also reflected when examining the defect energies of the various oxides, which are given in Table 2. Thus, all outer vacancies will be filled before the inner ones, even when a moderate electric field is applied. Moreover, this suggests a mechanism starting from a saturated (2×2) structure at 1/2 ML of oxygen such that the top rhodium layer would reconstruct to a hexagonal lattice [1], with oxygen atoms over it, leaving sites below it for subsurface oxygen to bind. Such a reconstructed surface could be a possible intermediate state before the formation of the trilayer.

3 Conclusions

In conclusion, we have investigated the initial steps in the oxidation on nano-sized rhodium facets in the presence of a high external electric field with field ion microscopy experiments (FIM) along with corresponding density functional theory (DFT) calculations on Rh(001), Rh(011) and Rh(111). We have demonstrated that for all three surface oxides the oxygen vacancies in the uppermost layer are thermodynamically unstable. The formation of an oxide was demonstrated through field ion microcopy experiments with the appearance of a cross-like granular structure when increasing the field from 11 V/nm to 12.3 V/nm. In addition, our density functional theory calculations show that an externally applied electric field can assist in the oxidation of a rhodium surface and that the corresponding changes in the activation barriers are in the range 0.001-0.1 eV/(V/nm) at moderate field values. These results imply that these surface oxides have a definite dependence on the external electric field and that it can be used as a tool to manipulate them.

4 Acknowledgements

TV and JSM (postdoctoral researchers) greatfully thank the Fond National de la Recherche Scientifique (FNRS) for financial support. This research is financially supported by the "Communauté française de Belgique" (contract "Actions de Recherche Concertées" No. 04/09-312).

[1] Such a reconstruction is known to occur on a Rh(011) surface when it is covered by 1/2 ML [29] of oxygen.

References

[1] C. Freysoldt, P. Rinke, M. Scheffler, Phys. Rev. Lett. **99** (2007) 086101.

[2] J. Gustafson, et al., Phys. Rev. Lett. **92** (2004) 126102.

[3] J. Gustafson, A. Mikkelsen, M. Borg, J. N. Andersen, Phys. Rev. B **71** (2005) 115442.

[4] C. Dri, C. Africh, F. Esch, G. Comelli, O. Dubay, L. Köhler, F. Mittendorfer, G. Kresse, J. Chem. Phys. **125** (2006) 094701.

[5] M. V. Ganduglia, K. Reuter, M. Scheffler, Phys. Rev. B **65** (2002) 245426.

[6] P. Dudin, A. Barinov, L. Gregoratti, M. Kiskinova, F. Esch, C. Dri, C. Africh, C. Comelli, J. Phys. Chem. B **109** (2005) 13649.

[7] J. Klikovits, M. Schmid, J. Gustafson, A. Mikklsen, A. Resta, E. Lundgren, J. Andersen, P. Varga, J. Phys. Chem. B **110** (2006) 9966.

[8] V. K. Medvedev, , Y. Suchorski, C. Voss, T. Visart de Bocarmé, T. Bär, N. Kruse, Langmuir **14** (1998) 6151.

[9] T. Visart de Bocarmé, G. Beketov, N. Kruse, Surf. Interface Anal. **36** (2004) 522.

[10] N. D. Lang, Solid State Commun. **7** (1969) 1047.

[11] Y. Suchorski, N. Ernst, W. Schmidt, V. K. Medvedev, H. J. Kreuzer, R. L. C. Wang, Prog. Surf. Sci. **53** (1996) 135.

[12] L. M. Sanders, R. Stumpf, T. R. Mattsson, B. S. Swartzentruber, Phys. Rev. Lett. **91** (2003) 206104.

[13] D. Tomanek, H. Kreuzer, J. Block, Surf. Sci. **157** (1985) L315.

[14] H. J. Kreuzer, Physics and chemistry in high electric fields, in: P. Avouris (Ed.), Atomic and nanometer-scale modification of materials, Kluwer academic publishing, Dordrecht, 1993, pp. 75–86.

[15] P. Gies, R. Gerhardts, Phys. Rev. B **33** (1985) 982.

[16] F. Schreier, F. Rebentrost, J. Phys. C: Solid State Phys. **20** (1987) 2069.

[17] M. R. Bassett, R. Imbihl, J. Chem. Phys. **93** (1990) 811.

[18] E. W. Müller, T. T. Tsong, Field Ion Microscopy, Principles and Applications, Elsevier, New York, 1969.

[19] K. D. Rendulic, M. Leisch, Surf. Sci. **95** (1980) L271.

[20] G. Kresse, J. Furthmüller, Phys. Rev. B **54** (1996) 11169.

[21] G. Kresse, J. Furthmüller, Computat. Mat. Sci. **6** (1996) 15.

[22] http://cms.mpi.univie.ac.at/vasp/.

[23] G. Kresse, D. Joubert, Phys. Rev. B **59** (1999) 1758.

[24] H. Jóhnsson, G. Mills, K. W. Jacobsen, Classical and Quantum Dynamics in Condensed Phase Simulations, World Scientific, Singapore, 1998.

[25] P. J. Feibelman, Phys. Rev. B **64** (2001) 125403.

[26] J.-S. McEwen, P. Gaspard, J. Chem. Phys. **125** (2006) 214707.

[27] J.-S. McEwen, P. Gaspard, T. Visart de Bocarmé, N. Kruse, In preparation.

[28] K. Reuter, Nanocatalysis: Principles, Methods, Case Studies, Springer, Berlin, 2006.

[29] G. Comelli, V. R. Dhanak, M. Kiskinova, K. Prince, R. Rosei, Surf. Sci Rep. **32** (1998) 165.

[30] J. P. Perdew, J. A. Chevary, S. H. Vosko, K. A. Jackson, M. R. Pederson, D. J. Singh, C. Fiolhais, Phys. Rev. B **46** (1992) 6671.